Abdominal Radiology (2019) 44:1246–1255
https://doi.org/10.1007/s00261-019-01958-9

SPECIAL SECTION: DISTINGUISHED PAPERS FROM JSAR

CT and MRI features of undifferentiated carcinomas with osteoclast-like giant cells of the pancreas: a case series

Yoshihiko Fukukura[1] · Yuichi Kumagae[1] · Mitsuho Hirahara[1] · Hiroto Hakamada[1] · Hiroaki Nagano[1] · Masanori Nakajo[1] · Kiyohisa Kamimura[1] · Masatoyo Nakajo[1] · Michiyo Higashi[2] · Takashi Yoshiura[1]

Published online: 27 February 2019

Abstract

Purpose The purpose of this case series was to describe computed tomography (CT) and magnetic resonance imaging (MRI) features of undifferentiated carcinoma with osteoclast-like giant cells of the pancreas.

Methods Institutional ethics review board approval was obtained, and informed consent was waived for this case series. We reviewed CT and MRI of patients with pathologically confirmed undifferentiated carcinoma with osteoclast-like giant cells of the pancreas found in the medical records of our hospital between 2006 and 2016.

Results Seven patients (3 males and 4 females; age, 59–82 years (mean, 71)) with confirmation by surgical resection ($n=3$) or biopsy ($n=4$) were identified. They underwent CT ($n=7$) and MRI ($n=6$). The tumors 26–83 mm in diameter (mean, 44 mm) were located in the head ($n=4$) or body ($n=3$) of the pancreas. They were demonstrated as lower attenuation areas relative to the adjacent pancreas on CT images obtained in both pancreatic and portal vein phases ($n=7$) with a well-defined smooth margin ($n=5$). They were demonstrated as hypointense areas relative to the pancreas on T2-weighted images ($n=4$) and T2*-weighted images ($n=4$) and diffusion-weighted images ($n=3$). They contained hemosiderin deposits on histology ($n=7$).

Conclusions Undifferentiated carcinoma with osteoclast-like giant cells of the pancreas might be present as low attenuation areas with a well-defined smooth margin on CT images obtained in pancreatic and portal vein phases, and hypointense areas on T2-, T2*-, and diffusion-weighted images caused by hemosiderin deposits.

Keywords Pancreatic neoplasm · Undifferentiated carcinoma · Multidetector computed tomography · Magnetic resonance imaging

Introduction

Pancreatic cancer is the fourth leading cause of cancer-related deaths in highly developed countries [1, 2]. Pancreatic ductal adenocarcinoma, which is the most common form of pancreatic cancer, has been well described in terms of computed tomography (CT) and magnetic resonance imaging (MRI) characteristics. Conversely, the CT and MRI characteristics of undifferentiated carcinoma of the pancreas are not well known.

Undifferentiated carcinoma of the pancreas is a malignant epithelial neoplasm in which a significant component of the neoplasm does not show a definitive direction of differentiation. It is considered a subtype of ductal carcinoma because ductal carcinoma components are found in most lesions [3–8]. This type of carcinomas can be further classified as anaplastic giant cell carcinoma, sarcomatoid carcinoma, and undifferentiated carcinoma with osteoclast-like giant cell types. Undifferentiated carcinoma with osteoclast-like giant cells is a rare neoplasm of the pancreas, accounting for just 1.4% of total pancreatic carcinomas [6]. There have been recent reports of this carcinoma suggesting that the clinical course might be better than conventional ductal carcinoma [6, 7, 9], although variable outcomes have been described [8]. However, little is known about the imaging features of

✉ Yoshihiko Fukukura
fukukura@m.kufm.kagoshima-u.ac.jp

[1] Department of Radiology, Kagoshima University Graduate School of Medical and Dental Sciences, 8-35-1 Sakuragaoka, Kagoshima 890-8544, Japan

[2] Human Pathology, Kagoshima University Graduate School of Medical and Dental Sciences, 8-35-1 Sakuragaoka, Kagoshima 890-8544, Japan

undifferentiated carcinoma with osteoclast-like giant cells, although several articles have been published on its pathology. The purpose of this case series was to describe the CT and MRI features of this carcinoma.

Materials and methods

Patient population

Institutional ethics review board approval was obtained, and informed consent was waived for this case series. We reviewed CT and MRI of patients with pathologically confirmed undifferentiated carcinoma with osteoclast-like giant cells of the pancreas found in the medical records of our hospital between 2006 and 2016.

CT imaging technique

CT was performed on a multidetector (16 or 64) row CT scanner using one of two CT units (Aquilion; Canon Medical Systems, Otawara, Japan). All scans began at the top of the liver and continued through to the end of the pancreas. The imaging parameters for all phases were as follows: tube voltage, 120 kVp; gantry rotation speed, 0.5 s; maximum allowable tube current, 440 mA; detector row configuration, 16 × 1 mm for 16-detector row CT or 64 × 0.5 mm for 64-detector row CT; and table increment, 15 mm/rotation for 16-detector row CT or 26.5 mm/rotation for 64-detector row CT. Pancreatic- and portal vein-phase images were obtained 23 s and 50 s after the bolus-tracking program detected the threshold aortic enhancement of 50 Hounsfield units. The scan delay for the delayed phase was fixed at 180 s after intravenous injection of 100 mL or 2 mL/kg body weight of nonionic contrast material with an iodine concentration of 300 mgI/mL (Omnipaque, Daiichi Sankyo, Tokyo, Japan) for a fixed duration of 30 s.

MRI technique

MRI was performed using a 1.5-T (Excelart Vantage, Canon Medical Systems, Otawara, Japan) or 3.0-T system (Ingenia, Philips, Best, Netherlands). The scan included a breath-hold gradient-echo T1-weighted and T2*-weighted images, a respiratory-triggered multishot turbo spin-echo image, a free-breathing single-shot echo-planar diffusion-weighted image with a b value of 800 or 1000 s/mm^2, and dynamic contrast-enhanced imaging before and after intravenous contrast injection of 0.025 mmol/kg body weight of gadoxetic acid (Primovist, Bayer Schering Pharma, Berlin, Germany) at a flow rate of one mL/s, followed by a 40-mL saline solution flush. Breath-hold three-dimensional fat-suppressed T_1-weighted gradient-echo imaging was repeated at 5 s (pancreatic phase), 45 s (portal vein phase), and 155 s (delayed phase) after the time of peak aortic enhancement, which was determined by the test injection. The MRI protocol and pulse sequence parameters are reported in Table 1.

Qualitative image analysis

Two radiologists (H.N. and Y.K., with 6 and 15 years of experience in abdominal radiology, respectively) independently evaluated all images. The following morphological features were carefully evaluated on CT: (a) tumor location (head, body, and tail), (b) TNM stage according to the International Union Against Cancer classification of pancreatic adenocarcinoma, (c) tumor margin (well-defined smooth and irregular), (d) interruption of the main pancreatic duct (MPD) indicated by upstream ductal dilatation (≥ 3 mm), (e) tumor thrombus in the portal venous system, (f) calcification, (g) tumor homogeneity (homogenous and heterogenous) on the portal vein phase-images, and (h) contrast enhancement relative to pancreatic parenchyma (low, iso, and high attenuation) on each phase of enhanced CT.

The readers were also asked to assess the following MRI characteristics: (a) predominant signal intensity relative to pancreatic parenchyma (low, iso, and high) on T1-, T2-, T2*-, and diffusion-weighted images; (b) hemorrhage, which was defined as a hyper intensity on T1-weighted image; (c) tumor homogeneity (homogenous or heterogeneous) on T2-weighted image; (d) cystic area on T2-weighted image; (e) capsule-like rim, which was defined as a low-intense rim on T2-weighted image; and (f) contrast enhancement relative to pancreatic parenchyma (low, iso, and high intensity) on each phase of contrast-enhanced image.

Any discrepancies were resolved during a third analysis by a third reader (Y.F., with 25 years of experience in abdominal radiology). The readers knew that the patients had pancreatic undifferentiated carcinoma with osteoclast-like giant cells, but were blinded to the results of the histopathological analyses.

Quantitative CT analysis

The tumor size and attenuation values of the tumor and pancreatic parenchyma during each CT phase were measured by a radiologist (H.H., with 13 years of experience in abdominal radiology) who did not participate in the qualitative imaging analysis and had no knowledge of the findings. The radiologist placed oval or circular regions of interest (ROIs) as large as possible within the tumor (mean size, 282 mm^2; range, 34–759 mm^2). Cystic, hemorrhagic, and calcified components in the tumor were excluded from the ROIs whenever possible. Attenuation values were measured for the normal pancreatic parenchyma adjacent to the pancreatic adenocarcinoma, while attempting to maintain a constant ROI area of

Table 1 MRI sequences and parameters

	T1WI		T2WI		T2*WI	DWI		Enhanced T1WI	
	1.5 T ($n=2$)	3.0 T ($n=4$)	1.5 T ($n=2$)	3.0 T ($n=4$)	3.0 T ($n=4$)	1.5 T ($n=2$)	3.0 T ($n=4$)	1.5 T ($n=1$)	3.0 T ($n=4$)
Repetition time (ms)	130	200	Respiratory intervals	Respiratory intervals	150	4000	6000	3.8	3.1
Echo time (ms)	4.8	2.4	90	80	7	70	50	1.4	1.5
Flip angle (°)	70	60	90	90	30	90	90	10	10
Echo train length	–	–	23	15	–	54	75	–	–
Parallel acquisition	2	2	1.8	2	2	2	2	2	2
b-value (s/mm^2)	–	–	–	–	–	800	1000	–	–
Field of view (mm^2)	320	350	320	350	350	320	350	350	320
Matrix (frequency × phase)	256 × 192	224 × 224	320 × 192	320 × 320	256 × 256	128 × 128	112 × 112	256 × 168	248 × 200
No. of sections acquired	20	30	20	30	30	20	30	40	60
Slice thickness / gap (mm)	9.0/1.0	5.0/0.5	9.0/1.0	5.0/0.5	5.0/0.5	9.0/1.0	5.0/0.5	5.0/0	3.2/0
No. of breath-hold	1	1	Free breathing	Free breathing	2	Free breathing	Free breathing	1	1

T1WI T1-weighted imaging, *T2WI* T2-weighted imaging, *T2*WI* T2*-weighted imaging, *DWI* diffusion-weighted imaging

approximately 1 cm^2. Visible blood vessels, pancreatic ducts, and artifacts were carefully excluded from the ROIs for pancreatic parenchyma.

Histopathological analysis

The final diagnosis was confirmed by a pathologist (M.H., with 24 years of experience in pathological evaluation) following surgical resection ($n=3$) or biopsy ($n=4$). The pathologist reported the percentages of hemosiderin containing histiocytic cells in each tumor, which were identified by hematoxylin and eosin stain and Perls' Prussian blue stain.

Statistical analysis

Statistical analyses were performed using the MedCalc Software (Mariakerke, Belgium). Kappa and weighted kappa analyses were used to determine interobserver agreement for the qualitative CT and MRI findings. The following cutoffs were used to indicate agreement: $\kappa=0.00$–0.20, slight agreement; $\kappa=0.21$–0.40, fair agreement; $\kappa=0.41$–0.60, moderate agreement; $\kappa=0.61$–0.80, substantial agreement and $\kappa=0.81$–1.00, almost perfect agreement [10].

Results

We identified 7 patients (3 males, 4 females; mean age, 71.1 years; range, 59–82 years) with pathologically confirmed undifferentiated carcinoma with osteoclast-like giant cells of the pancreas following surgical resection ($n=3$) or biopsy ($n=4$). The clinical findings of undifferentiated carcinoma with osteoclast-like giant cells are summarized in Table 2. The CT ($n=7$) and MRI results ($n=6$) are presented in Tables 3 and 4, respectively. Figure 1 shows the time attenuation curves of the tumors and pancreatic parenchyma.

Imaging revealed that the lesions were located in the head ($n=4$) or body ($n=3$) of the pancreas, with a maximum diameter of 26–83 mm (mean, 44.0 mm). Based on the UICC classification, one patient was in Stage IB, 3 patients were in Stage IIA, and 3 patients were in Stage IV. Enhanced CT showed a well-defined smooth tumor margin in 5 tumors (71.4%) (Figs. 2; 3). All tumors showed low attenuation relative to pancreatic parenchyma during the pancreatic and portal vein phases. Four tumors (57.1%) showed iso attenuation relative to pancreatic parenchyma

Table 2 Clinical features of seven cases of undifferentiated carcinoma with osteoclast-like giant cells

	No. patients
Sex	
Male	3
Female	4
Age	
Mean (years)	71.1 ± 6.6
Range (years)	59–82
Clinical manifestation	
Abdominal pain	2
Weight loss	1
Anemia	1
Appetite loss	1
No symptom	2
Serum amylase	
Elevated	1 (372 U/L)
Normal	6 (44–132 U/L)
Serum carbohydrate antigen 19-9	
Elevated	4 (37.5–1221.6 U/mL)
Normal	3 (< 37 U/mL)
Serum carcinoembryonic antigen	
Elevated	1 (11.3 ng/mL)
Normal	6 (< 5.68 ng/mL)

Data in parentheses are serum levels

Table 3 CT features of seven cases of undifferentiated carcinoma with osteoclast-like giant cells

CT features	Number
Tumor location	
Head	4
Body	3
Tail	0
Tumor size	
Mean (mm)	44.0 ± 17.5
Range (mm)	26–83
TNM stage	
I	1
II	3
IV	3
Tumor margin	
Well-defined smooth	5
Irregular	2
Main pancreatic duct interruption	
Present	6
Absent	1
Venous tumor thrombus	
Present	1
Absent	6
Calcification	
Present	1
Absent	6
Homogeneity	
Homogenous	1
Heterogenous	6
Contrast enhancement	
Attenuation of the tumor on pancreatic-phase images	
Low	7
Iso	0
High	0
Attenuation of the tumor on portal vein-phase images	
Low	7
Iso	0
High	0
Attenuation of the tumor on delayed-phase images	
Low	3
Iso	4
High	0

during the delayed phase. Interobserver agreements were moderate to almost perfect (κ values: 0.59–1.00).

The values (mean ± SD) of the tumors were 42.7 ± 4.9 HU on unenhanced CT. After contrast injection, the values were 75.0 ± 7.8 HU during the pancreatic phase, 74.9 ± 5.8 HU during the portal vein phase, and 73.6 ± 6.9 HU during the delayed phase.

Four tumors showed low intensity relative to pancreatic parenchyma on T2-weighted (66.7%) and T2*-weighted (100%) images (Figs. 2; 3). None of the tumors showed high intensity on diffusion-weighted imaging. On T2-weighted imaging, 4 of 6 tumors (66.7%) had a low-intense capsule-like rim (Fig. 3). Interobserver agreements were substantial to almost perfect (κ values: 0.67–1.00). All tumors showed low intensity relative to pancreatic parenchyma during all phases of contrast-enhanced imaging.

Surgical specimens from three patients showed well-marginated solid masses with a partially pseudo-capsule effect. Low-intense rim of one tumor on T2-weighted imaging corresponded to a relatively thick fibrous capsule. One tumor had cystic change on the cut surface corresponding to cystic area on T2-weighted imaging. The cut surfaces of solid tumors were dark reddish-brown and yellowish-white (Fig. 2). Histologic examination showed undifferentiated carcinoma comprising neoplastic pleomorphic mononuclear cells intermixed with abundant non-neoplastic osteoclast-like giant cells and histiocytic cells. All tumors were accompanied by hemosiderin deposition in the osteoclast-like giant cells and histiocytic cells (mean, 13.3%; range, 5–30%).

Table 4 MRI features of six cases of undifferentiated carcinoma with osteoclast-like giant cells

MR features	Number
The intensity of the tumor on T1-weighted images ($n=6$)	
Low	6
Iso	0
High	0
Hemorrhage on T1-weighted images ($n=6$)	
Present	1
Absent	5
The intensity of the tumor on T2-weighted images ($n=6$)	
Low	4
Iso	2
High	0
Homogeneity on T2-weighted images ($n=6$)	
Homogenous	1
Heterogenous	5
Cystic area on T2-weighted images ($n=6$)	
Present	1
Absent	5
Low-intense rim on T2-weighted images ($n=6$)	
Present	4
Absent	2
The intensity of the tumor on T2*-weighted images ($n=4$)	
Low	4
Iso	0
High	0
The intensity of the tumor on diffusion-weighted images ($n=6$)	
Low	3
Iso	3
High	0
Contrast enhancement ($n=5$)	
The intensity of the tumor on pancreatic-phase images	
Low	5
Iso	0
High	0
The intensity of the tumor on portal vein-phase images	
Low	5
Iso	0
High	0
The intensity of the tumor on delayed-phase images	
Low	5
Iso	0
High	0

Discussion

Despite increasing reports of undifferentiated carcinomas with osteoclast-like giant cells over the last decade, to the best of our knowledge, there is no comprehensive report describing the CT and MRI features of this pancreatic cancer type. The imaging features of undifferentiated carcinomas with osteoclast-like giant cells, as illustrated by individual case reports, are variable [11–16]. Therefore, the objective of the present study was to describe CT and MRI features of a series of pathologically proven undifferentiated carcinoma with osteoclast-like giant cells of the pancreas. According to our qualitative and quantitative findings, this carcinoma type can be characterized by well-defined solid tumors with low attenuation with prolonged enhancement on enhanced CT, low signal intensity on T2-, and T2*-weighted imaging, and low-to-iso intensity on diffusion-weighted imaging.

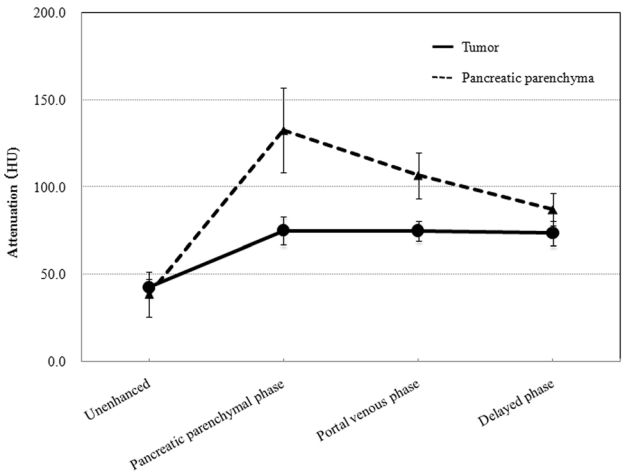

Fig. 1 Time attenuation curves of seven undifferentiated carcinomas with osteoclast-like giant cells and pancreatic parenchyma. The data points show the means and the error bars show the standard deviations of attenuation values of the tumor (black line) and pancreatic parenchyma (black dotted line). The mean attenuation values of the tumors and pancreatic parenchyma were 42.7 ± 4.9 and 38.8 ± 12.9 on the unenhanced CT; 75.0 ± 7.8 and 132.6 ± 24.2 on the pancreatic phase 74.9 ± 5.8 and 106.7 ± 13.3 on the portal vein phase; and 73.6 ± 6.9 and 87.1 ± 9.3 on the delayed phase, respectively

Previous case reports have described the CT appearance of undifferentiated carcinomas with osteoclast-like giant cells as a well-defined heterogeneous solid mass [11–14, 16]. In 6 patients (85.7%), an interruption of the MPD with upstream ductal dilatation was observed, which is consistent with previous reports [11, 13, 16] and is often seen as a secondary change in patients with pancreatic ductal adenocarcinoma [17–19]. Limited cases have been available regarding enhancement pattern of undifferentiated carcinomas with osteoclast-like giant cells, but variable enhancement patterns, such as hypo- [16] and hyperattenuation after contrast injection, have been reported [11, 14]. In our study, all tumors showed low attenuation relative to pancreatic parenchyma during the pancreatic and portal vein phases on enhanced CT. Thus, it may be difficult to differentiate between undifferentiated carcinomas with osteoclast-like giant cells and pancreatic ducal adenocarcinoma because

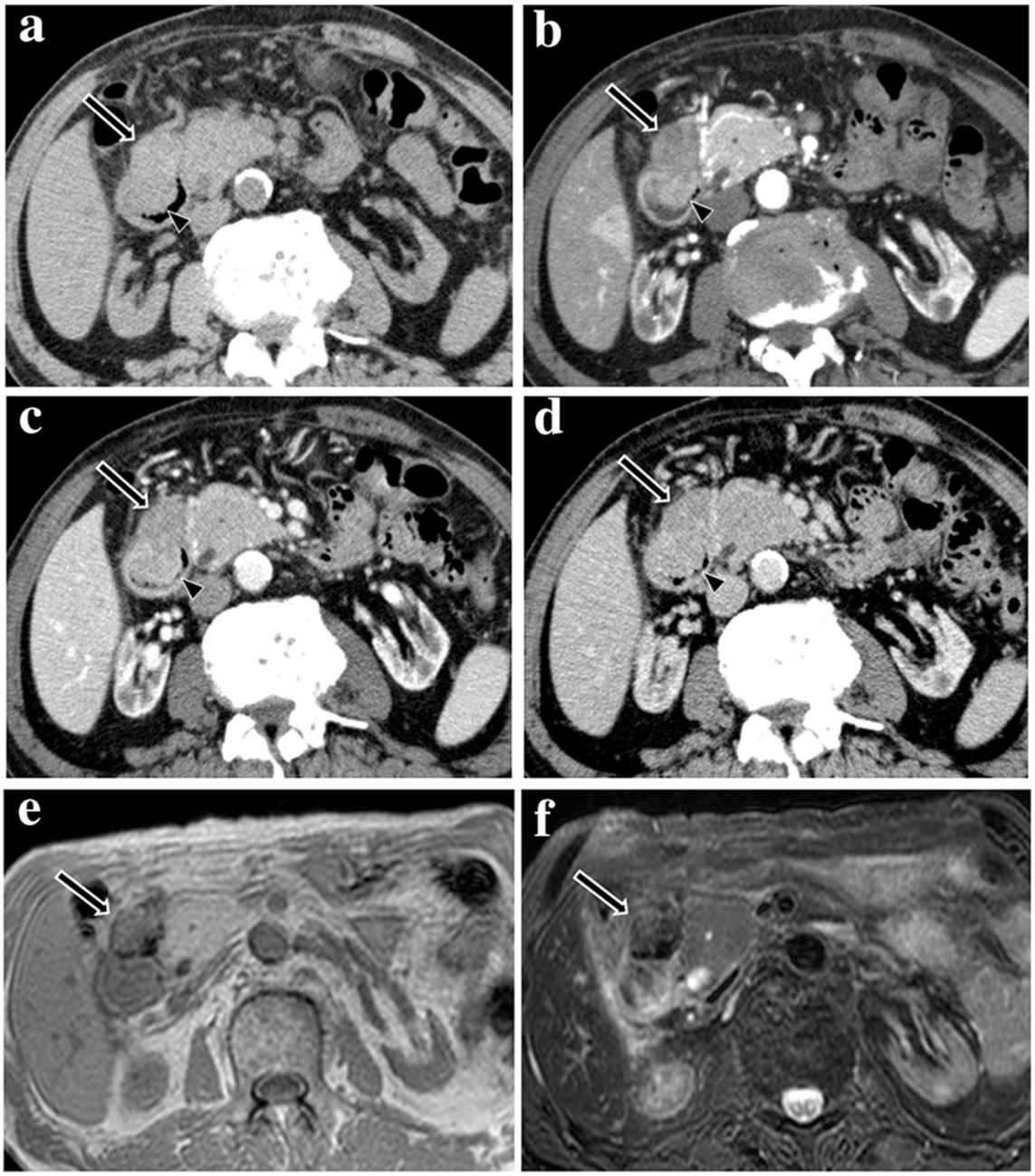

Fig. 2 A 74-year-old man with undifferentiated carcinoma with osteoclast-like giant cells with a tumor diameter of 39 mm in the pancreas head. Unenhanced CT showed a well-defined iso attenuating lesion (arrow) directly protruding into the adjacent duodenum (arrowhead) (**a**). The lesion (arrow) showed low attenuation relative to pancreatic parenchyma during the pancreatic (91 HU) (**b**) and portal vein phases (87 HU) (**c**), and iso attenuation during the delayed phase (78 HU) (**d**). On T1- (TR/TE, FA = 200/2.4, 60°) (**e**), fat-suppressed T2- (TR/TE = 1250/80) (**f**), T2*- (TR/TE, FA = 150/7.0, 30°) (**g**), and diffusion-weighted images (TR/TE = 6000/50, *b*-value = 1000 s/mm^2) (**h**), the lesion (arrow) showed heterogenous low intensity relative to pancreatic parenchyma. Grossly, the tumor was dark reddish-brown and partially infiltrated the adjacent duodenum (**i**). Histologically, it comprised atypical mononuclear cells with abundant osteoclast-like mononuclear giant cells and histiocytic mononuclear cells (Hematoxylin and eosin, × 200) (**j**). Perls' Prussian blue was expressed in the cytoplasm of giant cells and histiocytic cells (Perls' Prussian blue, × 200) (**k**)

the latter also tend to exhibit low attenuation during the pancreatic to portal vein phases of enhanced CT [17–19]. The tumors in our study, however, differed from pancreatic ductal adenocarcinoma, and showed a well-defined smooth tumor margin on enhanced CT in 5 tumors (71.4%), and a low-intense rim reflecting a fibrous capsule on T2-weighted imaging in 4 tumors (66.7%). Because the typical pancreatic ductal adenocarcinoma has an ill-defined irregular tumor

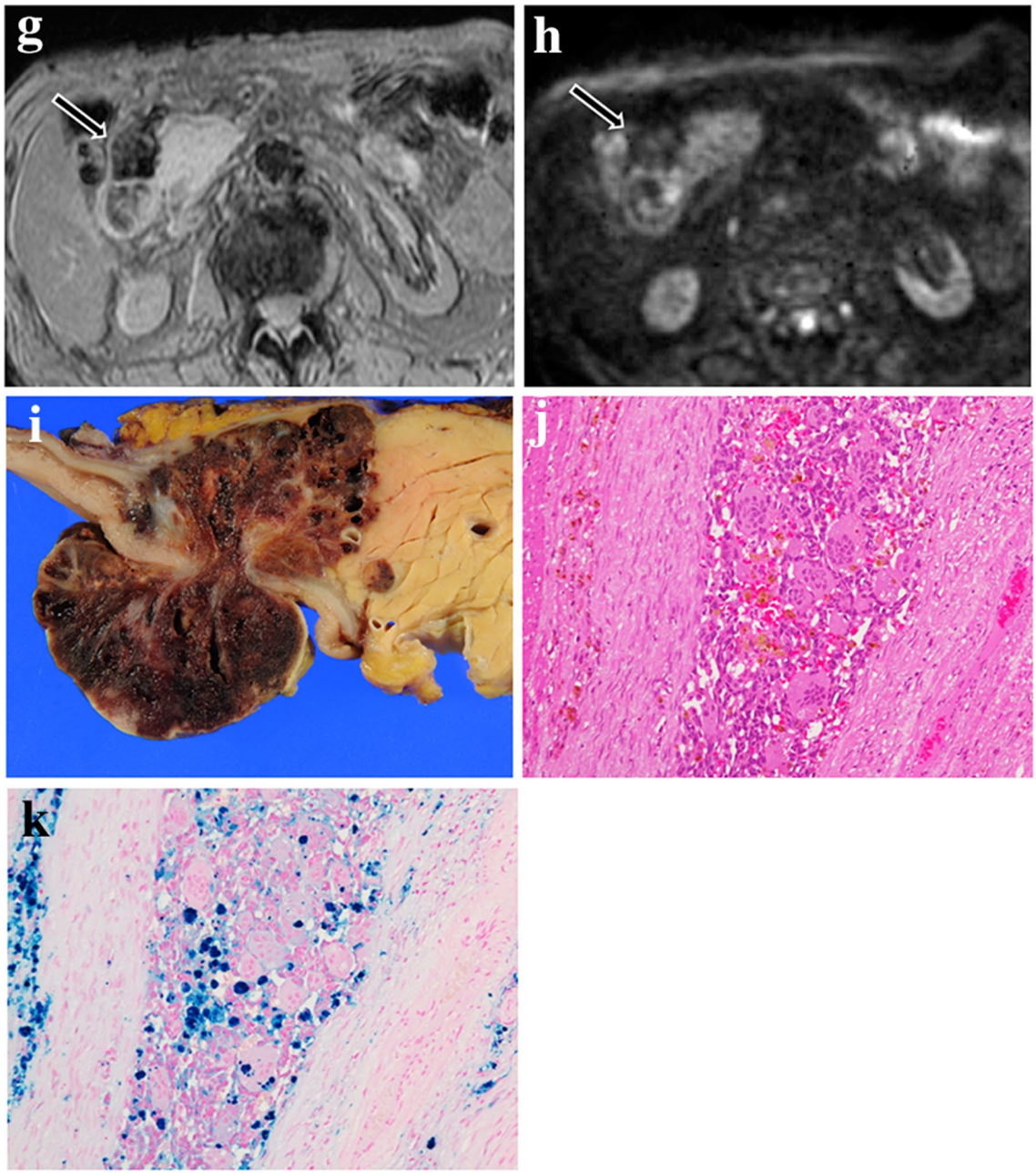

Fig. 2 (continued)

margin and is almost locally invasive, a well-defined smooth tumor margin can be used to distinguish undifferentiated carcinomas with osteoclast-like giant cells.

Most pancreatic ductal adenocarcinomas tend to show iso to low intensity on T1-weighted imaging and iso to high intensity on T2-weighted imaging [20–23]. To the best of our knowledge, there are no previous reports describing pancreatic ductal adenocarcinomas showing low intensity on T2- or T2*-weighted imaging. Few reports have described MRI appearance of undifferentiated carcinomas with osteoclast-like giant cells. In our study, the most frequent MRI findings were of low intensity on T1-, T2-, and T2*-weighted imaging, and no tumors showed high intensity on T2- or T2*-weighted imaging. Recognition of these MRI findings may thus be important for correctly diagnosing undifferentiated carcinoma with osteoclast-like giant cells.

Previous research has reported that most pancreatic ductal adenocarcinomas (80–97.5%) are completely or partially hyperintense on diffusion-weighted imaging [24]. In our study, all tumors showed low or iso intensity. This suggests that diffusion-weighted imaging might not be useful for delineating undifferentiated carcinoma with

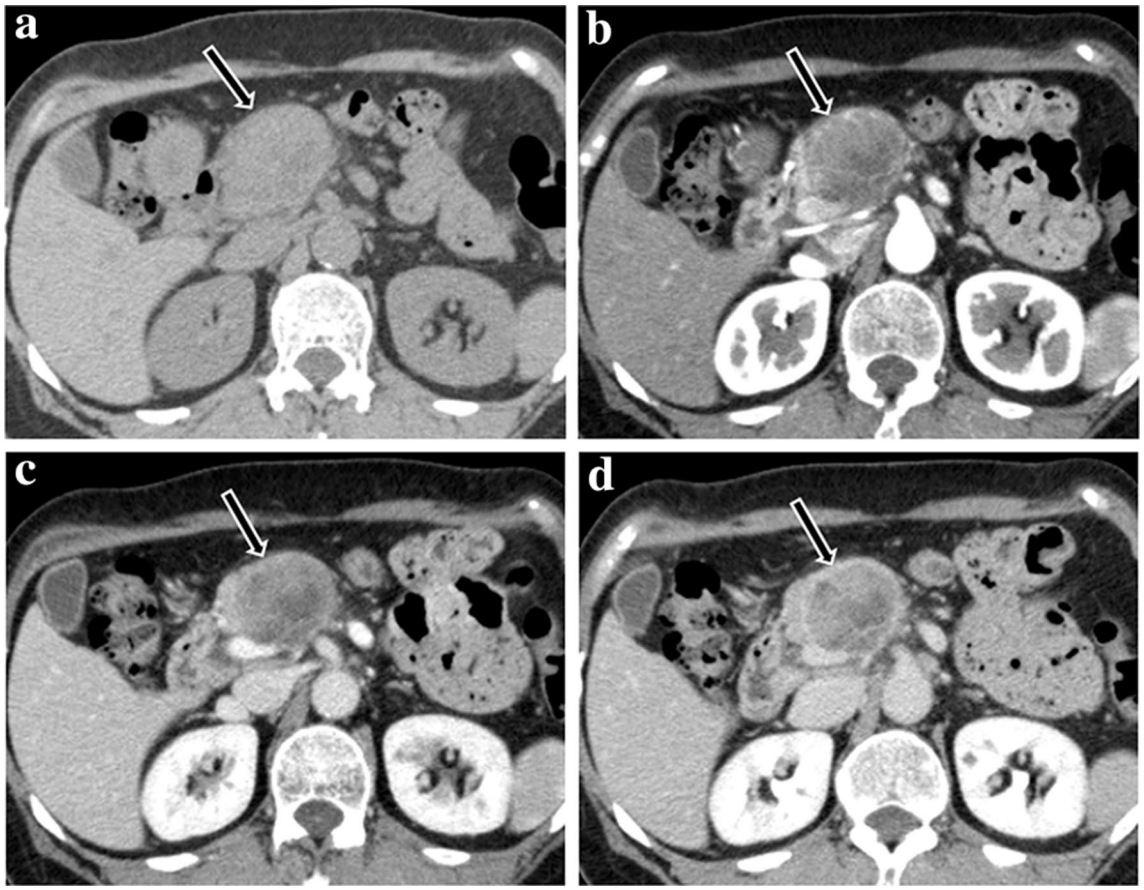

Fig. 3 A 59-year-old woman with undifferentiated carcinoma with osteoclast-like giant cells with a tumor diameter of 48 mm in the pancreas head. Quadriphasic axial CT showed a well-defined solid lesion with heterogenous enhancement. The lesion (arrow) showed iso attenuation (46 HU) on unenhanced CT (**a**) and low attenuation during the pancreatic (74 HU) (**b**), portal vein (70 HU) (**c**), and delayed phases (62 HU) (**d**). T1-weighted imaging (TR/TE, FA = 200/2.4, 60°) (**e**) revealed a heterogeneous mild low-intense lesion (arrow) with spotty high intensity reflecting hemorrhage. Fat-suppressed T2-weighted imaging (TR/TE = 1140/80) showed a heterogenous low-intense lesion (arrow) with low-intense rim reflecting the fibrous capsule (**f**). On fat-suppressed T2- (TR/TE = 1140/80) (**f**), T2*- (TR/TE, FA = 150/7.0, 30°) (**g**), and diffusion-weighted images (TR/TE = 6000/50, *b*-value = 1000 s/mm^2) (**h**), the lesion (arrow) showed heterogenous low intensity relative to pancreatic parenchyma

osteoclast-like giant cells, and that other MR sequences, such as T1-weighted, T2-weighted, and contrast-enhanced imaging, may be required.

Various pathologies can account for a decreased signal on T2-, T2*-, and diffusion-weighted imaging, including hemosiderin, dense fibrosis, hyalinization, necrosis calcification/ossification, and artifacts. Undifferentiated carcinomas with osteoclast-like giant cells are histologically composed of highly pleomorphic neoplastic mononuclear cells and large non-neoplastic multinucleated osteoclast-like giant cells. Some of the mononuclear cells are atypical, while others can be histiocyte-like. Osteoclast-like giant cells and mononuclear histiocytic cells can be phagocytically active and may contain hemosiderin [4, 5]. In our study, tumors were grossly dark reddish-brown and histologically associated with abundant osteoclast-like giant cells and histiocytic cells. We confirmed varying hemosiderin deposits in the osteoclast-like giant cells and histiocytic cells of all tumors. Other possible causative findings corresponding to low-intensity appearances were not histologically observed in our tumors. Thus, abundant hemosiderin deposition in tumors is thought to lead to a decreased signal on T2-, T2*-, and diffusion-weighted imaging.

Previous case reports have described cystic change [14], hemorrhage [12, 13], and calcification [12] within undifferentiated carcinomas with osteoclast-like giant cells and venous tumor thrombus [13]. Although most of the tumors in this study showed heterogenous enhancement, each finding (presence of cystic area, hemorrhage, or calcification) was observed in only one patient. A larger study is required to clarify whether these findings are characteristic of undifferentiated carcinoma with osteoclast-like giant cells.

This study is subject to several limitations. First, a relatively small number of patients were included, which

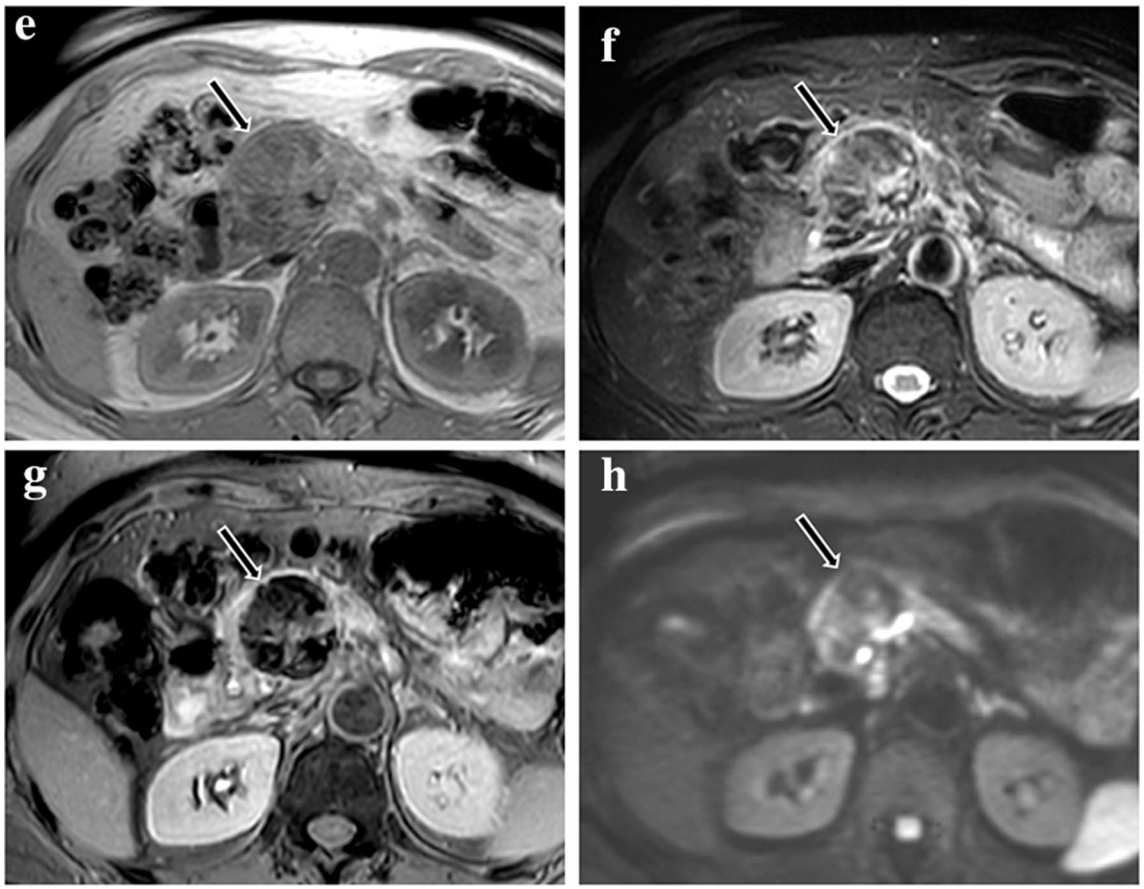

Fig. 3 (continued)

reflects the rarity of this carcinoma type. Second, there was variability in the imaging parameters because of the substantial changes in imaging technology that occurred during the 10-year study period. Third, all lesions were undifferentiated carcinomas with osteoclast-like giant cells of the pancreas, and no other pancreatic pathologies were included in the present study. Bias might therefore have existed in the interpretation of CT and MRI.

In conclusion, most undifferentiated carcinomas with osteoclast-like giant cells had a well-defined, hypovascular, and low-intensity appearance on T2- and T2*-weighted imaging, and showed iso to low intensity on diffusion-weighted imaging. The low-intensity appearance likely results from hemosiderin deposits in the abundant histiocytic cells of the tumors. Recognition that undifferentiated carcinomas with osteoclast-like giant cells have a well-defined hypovascular appearance with a decreased signal on MRI may be helpful in differentiating them from other pancreatic solid lesions.

Funding There was no financial support for this study.

Compliance with ethical standards

Conflict of interest The authors declare that they have no conflict of interest.

Ethical approval Institutional ethics review board approval was obtained and informed consent was waived for this retrospective study.

References

1. Willett CG, Czito BG, Bendell JC, Ryan DP (2005) Locally advanced pancreatic cancer. J Clin Oncol 23:4538–4544
2. Malvezzi M, Bertuccio P, Levi F, La Vecchia C, Negri E (2014) European cancer mortality predictions for the year 2014. Ann Oncol 25:1650–1656
3. Molberg KH, Heffess C, Delgado R, Albores-Saavedra J (1998) Undifferentiated carcinoma with osteoclast-like giant cells of the pancreas and periampullary region. Cancer 82:1279–1297
4. Sakai Y, Kupelioglu AA, Yanagisawa A, et al. (2000) Origin of giant cells in osteoclast-like giant cell tumors of the pancreas. Hum Pathol 31:1223–1229
5. WHO (2010) *WHO classification of tumours of the digestive system*. Lyon: PIARC Press, pp 322–326

6. Muraki T, Reid MD, Basturk O, et al. (2016) Undifferentiated carcinoma with osteoclastic giant cells of the pancreas: clinicopathologic analysis of 38 cases highlights a more protracted clinical course than currently appreciated. Am J Surg Pathol 40:1203–1216
7. Luchini C, Pea A, Lionheart G, et al. (2017) Pancreatic undifferentiated carcinoma with osteoclast-like giant cells is genetically similar to, but clinically distinct from, conventional ductal adenocarcinoma. J Pathol 243:148–154
8. Reid MD, Muraki T, HooKim K, et al. (2017) Cytologic features and clinical implications of undifferentiated carcinoma with osteoclastic giant cells of the pancreas: an analysis of 15 cases. Cancer Cytopathol 125:563–575
9. Strobel O, Hartwig W, Bergmann F, et al. (2011) Anaplastic pancreatic cancer: presentation, surgical management, and outcome. Surgery 149:200–208
10. Landis Koch GG (1977) The measurement of observer agreement for categorical data. Biometrics 33:159–174
11. Shindoh N, Ozaki Y, Kyogoku S, et al. (1998) Osteoclast-type giant cell tumor of the pancreas: helical CT scans. AJR Am J Roentgenol 170:653–654
12. Ichikawa T, Federle MP, Ohba S, et al. (2000) Atypical exocrine and endocrine pancreatic tumors (anaplastic, small cell, and giant cell types): CT and pathologic features in 14 patients. Abdom Imaging 25:409–419
13. Togawa Y, Tonouchi A, Chiku T, et al. (2010) A case report of undifferentiated carcinoma with osteoclast-like giant cells of the pancreas and literature review. Clin J Gastroenterol 3:195–203
14. Sah SK, Li Y, Li Y (2015) Undifferentiated carcinoma of the pancreas with osteoclast-like giant cells: a rare case report and review of the literature. Int J Clin Exp Pathol 8:11785–11791
15. Toshima F, Inoue D, Yoshida K, et al. (2016) Adenosquamous carcinoma of pancreas: CT and MR imaging features in eight patients, with pathologic correlations and comparison with adenocarcinoma of pancreas. Abdom Radiol 41:508–520
16. Yang KY, Choi JI, Choi MH, et al. (2016) Magnetic resonance imaging findings of undifferentiated carcinoma with osteoclast-like giant cells of pancreas. Clin Imaging 40:148–151
17. Kim JH, Park SH, Yu ES, et al. (2010) Visually isoattenuating pancreatic adenocarcinoma at dynamic-enhanced CT: frequency, clinical and pathologic characteristics, and diagnosis at imaging examinations. Radiology 257:87–96
18. Yoon SH, Lee JM, Cho JY, et al. (2011) Small (</=20 mm) pancreatic adenocarcinomas: analysis of enhancement patterns and secondary signs with multiphasic multidetector CT. Radiology 259:442–452
19. Fukukura Y, Takumi K, Higashi M, et al. (2014) Contrast-enhanced CT and diffusion-weighted MR imaging: performance as a prognostic factor in patients with pancreatic ductal adenocarcinoma. Eur J Radiol 83:612–619
20. Gabata T, Matsui O, Kadoya M, et al. (1994) Small pancreatic adenocarcinomas: efficacy of MR imaging with fat suppression and gadolinium enhancement. Radiology 193:683–688
21. Yu MH, Lee JY, Kim MA, et al. (2010) MR imaging features of small solid pseudopapillary tumors: retrospective differentiation from other small solid pancreatic tumors. AJR Am J Roentgenol 195:1324–1332
22. Jang KM, Kim SH, Kim YK, et al. (2012) Imaging features of small (≤3 cm) pancreatic solid tumors on gadoxetic-acid-enhanced MR imaging and diffusion-weighted imaging: an initial experience. Magn Reson Imaging 30:916–925
23. Park MJ, Kim YK, Choi SY, et al. (2014) Preoperative detection of small pancreatic carcinoma: value of adding diffusion-weighted imaging to conventional MR imaging for improving confidence level. Radiology 273:433–443
24. Fukukura Y, Takumi K, Kamimura K, et al. (2012) Pancreatic adenocarcinoma: variability of diffusion-weighted MR imaging findings. Radiology 263:732–740